

Article

The Mechanism of Casing Deformation before Hydraulic Fracturing and Mitigation Measures in Shale Gas Horizontal Wells

Yisheng Mou ^{1,*}, Jian Cui ², Jianjun Wu ³, Fengqi Wei ⁴, Ming Tian ⁵ and Lihong Han ^{1,*}

¹ State Key Laboratory for Performance and Structure Safety of Petroleum Tubular Goods and Equipment Materials, CNPC Tubular Goods Research Institute, Xi'an 710077, China

² Changqing Branch, CNPC China National Logging Corporation, Xi'an 710201, China

³ CNPC Coalbed Methane Company Limited, Beijing 100028, China

⁴ CNPC Exploration and Production Company, Beijing 100007, China

⁵ CNPC Tarim Oilfield Company, Korla 841000, China

* Correspondence: mouys@cnpc.com.cn (Y.M.); hanlihong@cnpc.com.cn (L.H.)

Abstract: During the development of shale gas, one of the major challenges is the casing deformation (CD) in the horizontal section due to the geological activity. Recently, the casing deformation before hydraulic fracturing (CDBF) occurred in multiple shale gas wells in L block in China. In this paper, based on the theory of tubular mechanics, the relationship between casing buckling and CDBF caused by casing running in is analyzed qualitatively and quantitatively. It is found that the buckling deformation caused by running the casing string process is not sufficient to prevent the tool ($\Phi 99$ mm bridge plug). On the other hand, the mechanism of CDBF is systematically analyzed based on the actual field data and finite element (FE) method. In order to analyze the CDBF mechanism, the comparison between the actual casing trajectory and the reservoir rock (S#1, S#2, S#3 and M#1) in horizontal section in H2 platform is carried out, and the preliminary CDBF mechanism is proposed. Then, two groups of FE models are established to reduce the CD process to verify the preliminary mechanism. It is found that the numerical simulation results (high stress section length from FE model) are in good agreement with the actual CD logging results. Based on the analytical results, the corresponding mitigation measures are proposed based on the analysis of the CDBF mechanism. Our work could offer a detailed theoretical basis and reference of CDBF for shale gas well application.

Keywords: casing deformation; casing string; tubular mechanics; shale gas well; fracturing



Citation: Mou, Y.; Cui, J.; Wu, J.; Wei, F.; Tian, M.; Han, L. The Mechanism of Casing Deformation before Hydraulic Fracturing and Mitigation Measures in Shale Gas Horizontal Wells. *Processes* **2022**, *10*, 2612. <https://doi.org/10.3390/pr10122612>

Academic Editor: Wei-Hsin Chen

Received: 25 October 2022

Accepted: 28 November 2022

Published: 6 December 2022

Publisher's Note: MDPI stays neutral with regard to jurisdictional claims in published maps and institutional affiliations.



Copyright: © 2022 by the authors. Licensee MDPI, Basel, Switzerland. This article is an open access article distributed under the terms and conditions of the Creative Commons Attribution (CC BY) license (<https://creativecommons.org/licenses/by/4.0/>).

1. Introduction

Currently, the provision of conventional oil and gas resources cannot meet the rapid growth of energy consumption [1]. Hence, the development of unconventional reservoirs has drawn growing attention from energy companies [2]. As a high-quality, efficient and clean low-carbon primary energy source, shale gas has been increasingly favored and valued by all countries in the world [3–5]. In order to effectively increase production and efficiency, large-scale and high-pump pressure fracturing technology has been applied to the development of deep shale gas reservoirs and achieved considerable results [6].

It is worth noting that although fracturing technology has improved the efficiency of shale gas production, problems such as high construction pressure and asymmetric transformation area in the fracturing process frequently lead to wellbore structural damage and destruction. The non-uniform fracture expansion after fracturing will seriously interfere with the stress state of casing and lead to casing deformation (CD) [7]. According to statistics, 32 wells of the Marcellus shale gas field in the United States suffered from CD under fracturing, while 28 wells of the Quebec shale gas field in Canada suffered from different types of casing damage and failure deformation during large-scale fracturing [8]. In China,

the CD of shale gas wells is even worse. Among 141 wells fractured in Changning-Weiyuan, 36 wells have casing damage with 48 deformation points [9]. CD seriously affects the safety of shale gas wells and even leads to the abandonment of wells in advance.

With the emergence of CD in early shale gas wells, many scholars have carried out analysis and research on the CD of shale gas. Daneshy et al. [10] analyzed the geological factors in the fracturing process of shale gas by means of numerical simulation, and believed that the formation shear failure and unbalanced deformation were the main reasons leading to CD. Sugden et al. [11] concluded that CD failure in shale gas wells is the result of various comprehensive factors such as complex borehole trajectory, multi-stage high-displacement fracturing and temperature variation. Lian et al. [12] established the finite element model of CD failure during multi-stage hydraulic fracturing based on the micro-seismic surveillance data, theories of fracture mechanics, rock damage mechanics and rock failure criterion, and studied the influence of in-situ stress deficit on CD. Li et al. [13] used 3D imaging analysis software and diameter measurement data to conduct 3D imaging modeling for severe CD of two shale gas horizontal wells, and obtained morphological characteristics of deformed casing. Yan et al. [14] established the physical model and finite element model of fracturing CD for high in-situ stress shale gas. The influences of pore angle, temperature variation, internal pressure and ground stress on CD have been studied. Fei et al. [15] carried out quantitative research on hydraulic fracturing induced fracture slip and CD in shale gas wells, finding that hydraulic fracturing could cause fracture slip and casing shear deformation, and suggested that the perforation should be far away from the weak interface. Xi et al. [16] proposed a new investigation on casing shear deformation during multistage fracturing in shale gas wells based on microseism data, and established a mathematical model of the relationship between microseismic moment magnitude and slip distance, which was verified by physical model experiments. Guo et al. [17] studied the volumetric fracturing CD of horizontal shale gas wells by numerical simulation, discussed the influences of fault slippage on casing stress and displacement and found that fault slippage is an important mechanism of CD near the heel. Holt et al. [18] carried out the triaxial failure tests, creep tests and tests tailored to follow the failure envelope under simulated borehole conditions, and found that the stress history and possibly cementation are keys in determining the failure mode. Li et al. [19] studied the CD mechanisms of horizontal wells in shale gas fields during multistage hydraulic fracturing by numerical simulations, discussing the influence of different factors such as shale expansion, injection pressure and formation mechanical properties on CD. Ajayi et al. [20] used derived equations to conduct parametric studies of specific transport conditions to understand the influence of stratum geology, fracture lengths, and the leaked gas properties on subsurface transport, and found that the prediction that the subsurface gas flux decreases with an increase in fracture length is specifically for a non-gassy stratum. Yang et al. [21] studied the failure mode and mechanism of casing in shale gas wells of Sichuan-Chongqing, designed and developed a set of experimental equipment for testing CD and failure of different casing materials under different loads, and put forward a model for predicting the maximum allowable stress of casing. Mohammed et al. [22] proposed an application of FE analysis and machine learning for the prediction and optimization of casing buckling and deformation responses in shale gas wells in an in-situ operation, and studied the effects of combined loading using multiple parameters on stress, displacement and final casing safety factors, as well as the relationship between each parameter. Lu et al. [23] established a prediction model for hydraulic fracturing induced casing shear deformation and CD based complex function, and discussed the factors affecting wellbore shear stress and CD.

Despite some valuable work on CD in shale gas wells, most previous studies focus on establishing a model of CD using numerical simulation methods; meanwhile, there are few reports on the phenomenon of casing deformation before hydraulic fracturing (CDBF). In this paper, based on the theory of tubular mechanics, the relationship between casing buckling and CDBF caused by casing running is analyzed qualitatively and quantitatively.

Moreover, the mechanism of CDBF is systematically analyzed based on the actual field data and FE method.

2. Case Introduction

According to the time stage of CD, two forms of CD are distinguished: (i) CDBF, (ii) casing deformation after hydraulic fracturing (CDAF). Compared to CDAF, CDBF has a more negative impact on oil and gas production, because it directly caused the perforation procedure to fail, which severely affected engineering performance. Figure 1 illustrates the schematic of the general process of CDBF in M block: (i) casing rotation is widely used to reduce friction in horizontal wells (Figure 1a); the casing is rotated and run into the well bottom in drilling mud, rotation speed is 10~30 rpm, and running speed is 10~25 m/min. (ii) when the casing is run into the designed well depth, the known points A and B are determined in horizontal section of wells, as can be seen in Figure 1b, (iii) Figure 1c shows the process of cementing, (iv) after waiting for cement setting, the downhole tool (e.g., bridge plug and perforating gun) is run into the well but, unfortunately, the tool cannot pass through the casing because of CDBF, as shown in Figure 1d.

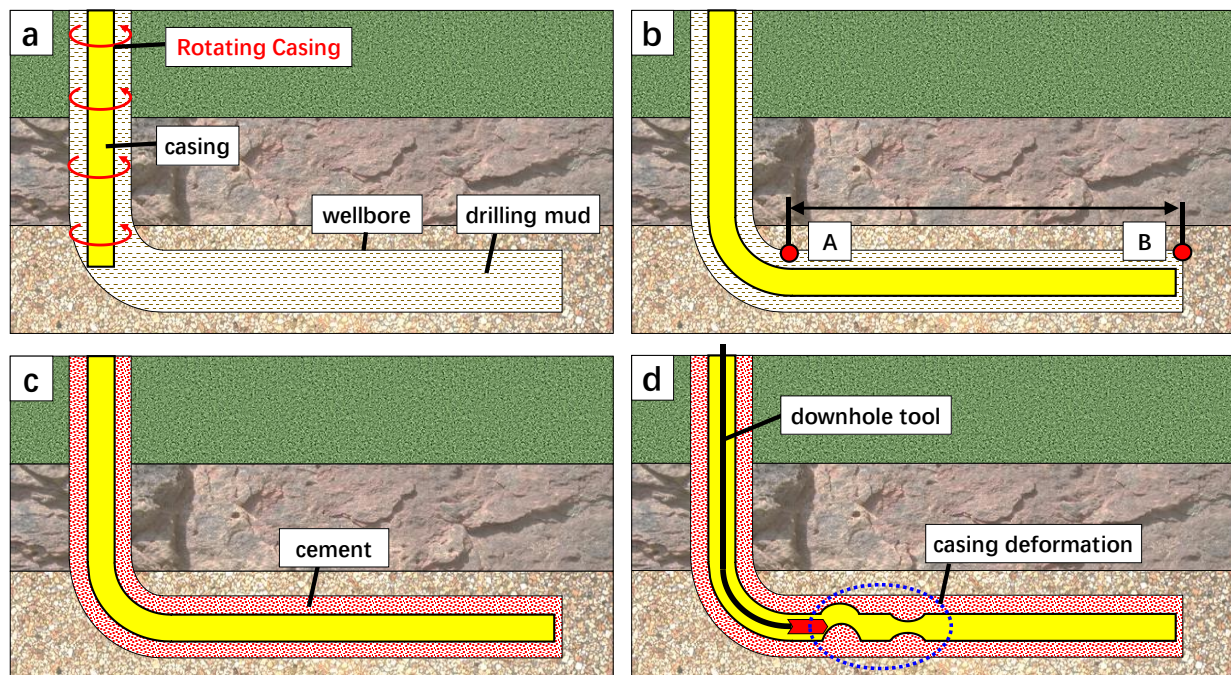


Figure 1. The schematic diagram of the CDBF process: (a) Casing run process, (b) A-B section is determined, (c) cementing, (d) tool is blocked.

Recently, CD occurred in multiple shale gas wells in L block in China; it is worth noting that CDBF has become a new problem. Figure 2 illustrates the statistics on the number of CD wells and the types of CD positions. Significantly, the percentage of CD wells (CDBF and CDAF) has reached 62.51%; meanwhile, the percentage of wells with CDBF is already high, at 34.38%. Moreover, shear deformation is the predominant type among CDBF wells (shear type is 72.22%, flattening type is 23.53%, complex type is 4.25%).

In this work, to further study the mechanism of CDBF, the H2 platform is used as a case study because of the typical CDBF phenomenon in its four wells. Figure 3 presents the distribution of the natural fractures/faults and borehole trajectories near the H2 platform. These fractures/faults formed naturally before the drilling process, and they are measured using a downhole micro-seismic method. Meanwhile, Table 1 illustrates the information statistics for four wells in the H2 platform.

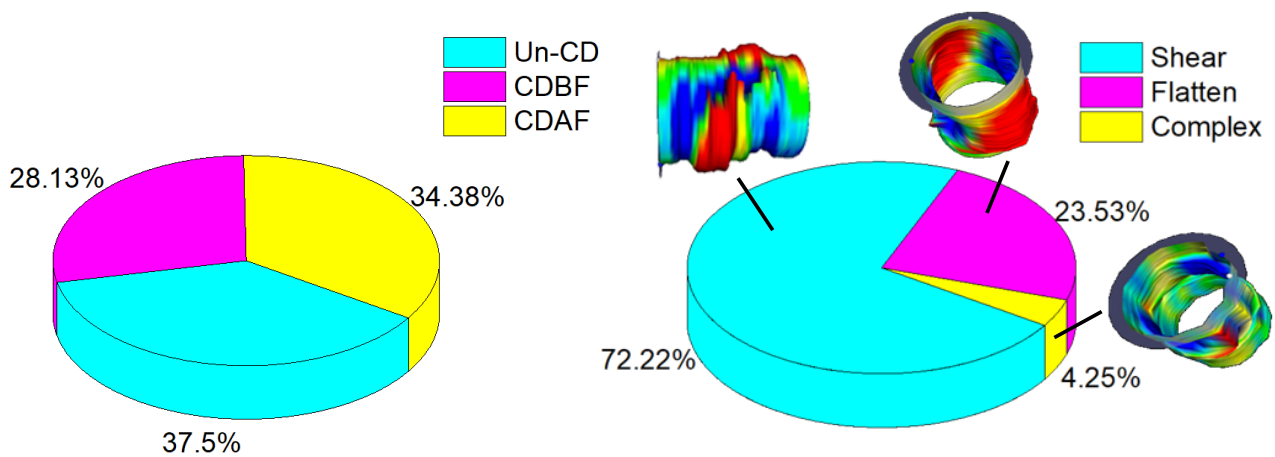


Figure 2. The statistics on the number of CD wells and the types of CD positions in L block.

From the borehole trajectory perspective, it can be seen that: (i) the measured depth of the four wells are 5944.85 m, 5920.00 m, 5954.61 m and 6051.67 m respectively, (ii) the max dogleg severity of the four wells are 7.50°/30 m, 7.07°/30 m, 7.89°/30 m and 6.93°/30 m respectively, (iii) the horizontal section lengths of the four wells are 1735 m, 1759 m, 1785 m and 1780 m, respectively (the starting position of the horizontal section is defined as A location, the end of the horizontal section is defined as B location), (iv) the borehole trajectory of the horizontal section of each well traverses at least 5 fractures/faults (5 times in H2-1, 5 times in H2-2, 6 times in H2-3 and 8 times in H2-4).

Moreover, from the production casing perspective, it can be seen that: (i) the casing size in each well is $\Phi 139.7 \times T12.7$ —steel degree 140 ksi (965 MPa), with the casing centralizer scheme as presented in Table 1; (ii) the running method of each well is casing rotating (20 rpm, 11 m/min), the mud density is 2.09 g/cm³, the temperature gradient of the stratum is 2.73 °C/100 m, and the pore pressure gradient of the stratum is 0.997 MPa/100 m; (iii) according to the logging results, CDBF occurred in H2-1, H2-3 and H2-4, and the locations of CD position are shown in Table 1.

In the geology perspective, adjacent to H2 platform are H1 platform and H3 platform, both of which have been fractured.

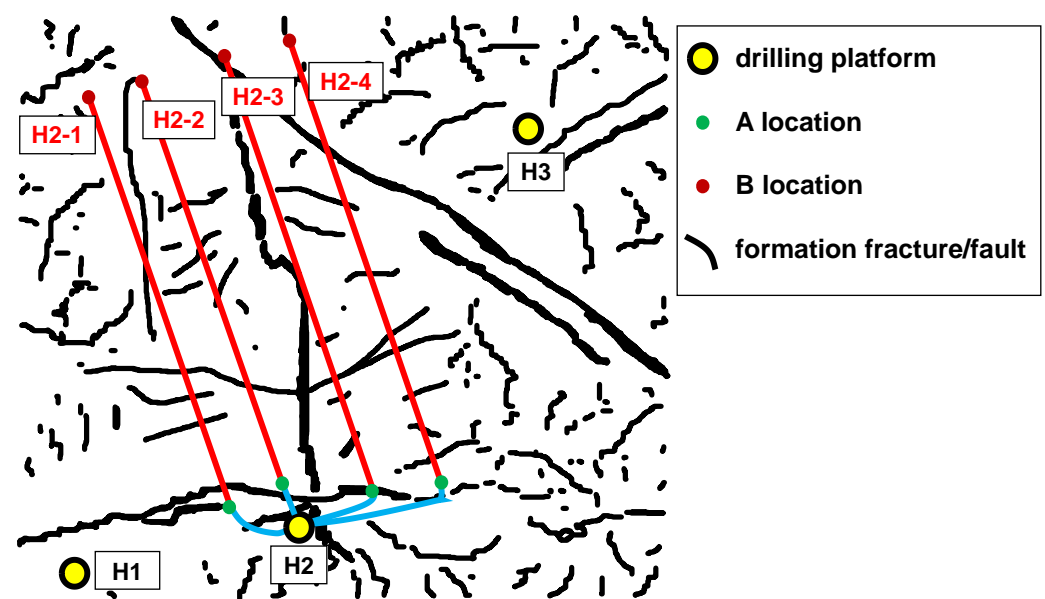


Figure 3. The distribution of the natural fractures/faults and borehole trajectories near the H2 platform.

Table 1. The information statistics for four wells in the H2 platform.

No.	CD Mold	Measure Depth (m)	Max Dogleg Severity (°/30 m)	Horizontal Section Length (m)	Running Method	Casing Centralizer Scheme	CD Posion (m)
H2-1	CDBF	5944.85	7.50	1735			4309.32–4314.76
							4356.01–4356.49
							4377.48–4378.79
H2-2	/	5920.00	7.07	1759			/
H2-3	CDBF	5954.61	7.89	1785	Casing rotating 20 rpm 11 m/min	spaced 11 m apart Rigid Φ205 mm	4146.36–4149.07
							4269.99–4273.49
							4373.04–4377.96
							4399.85–4401.99
							4605.50–4606.37
H2-4	CDBF	6051.67	6.93	1780			4263.40–4265.00
							4340.60–4343.60
							4481.50–4483.50
							4552.30–4553.30

3. Casing String Buckling and Passability

3.1. Buckling

It is well known that the running process of the tool inside the string could be blocked if the degree of the string buckling exceeds a certain level. Meanwhile, the casing string buckling is easily caused during running the string in the borehole because of the large friction resistance in shale gas horizontal wells. According to the actual operating parameters (Table 1) and the theory of tubular mechanics, the present study on the buckling deformation of the four wells of H2 platform is carried out as follows.

From the mechanical perspective, during running the string process in, the accumulation of the total internal forces ΔF_{all} in the structure could be mainly caused by the effect of the large friction force ΔF_1 due to well trajectory and string effective weight. Meanwhile, the internal force of the casing string is also affected by the buckling effect ΔF_2 , the friction effect due to fluid flow ΔF_3 , the ballooning effect ΔF_4 , and the piston effect ΔF_5 in horizontal wells. The total internal forces ΔF_{all} of the casing string could be calculated by different effects, as shown in Equation (1) [24]. In our work, these effects are taken into account to calculate the mechanical behavior of the whole section casing string.

$$\Delta F_{all} = \Delta F_1 + \Delta F_2 + \Delta F_3 + \Delta F_4 + \Delta F_5 \quad (1)$$

When the total internal forces ΔF_{all} exceeds the critical load of string buckling, the buckling of the string could be caused. Figure 4 presents the lateral deformation displacement of casing strings in four wells vs. measured depth: (a) H2-1, (b) H2-2, (c) H2-3, (d) H2-4. In the figure, 0~180° is the high position of the wellbore, which indicates the casing position relative to the high or low side of the bore; meanwhile, 90~270° is the right position of the wellbore, which indicates the casing position relative to the left or right side of the bore, and wellbore is the wellbore boundary, which limits the degree of lateral deformation of the casing. It can be seen from Figure 4 that the buckling casing has a high frequency of deformation along measured depth, but little horizontal displacement (the horizontal displacement of the buckling casing is only ±5.5 mm) along the borehole trajectory. The use of centralizer plays an active role in reducing the buckling deformation of casing. Therefore, the passability of the bridge plug must be negatively affected according to the buckling deformation of casing.

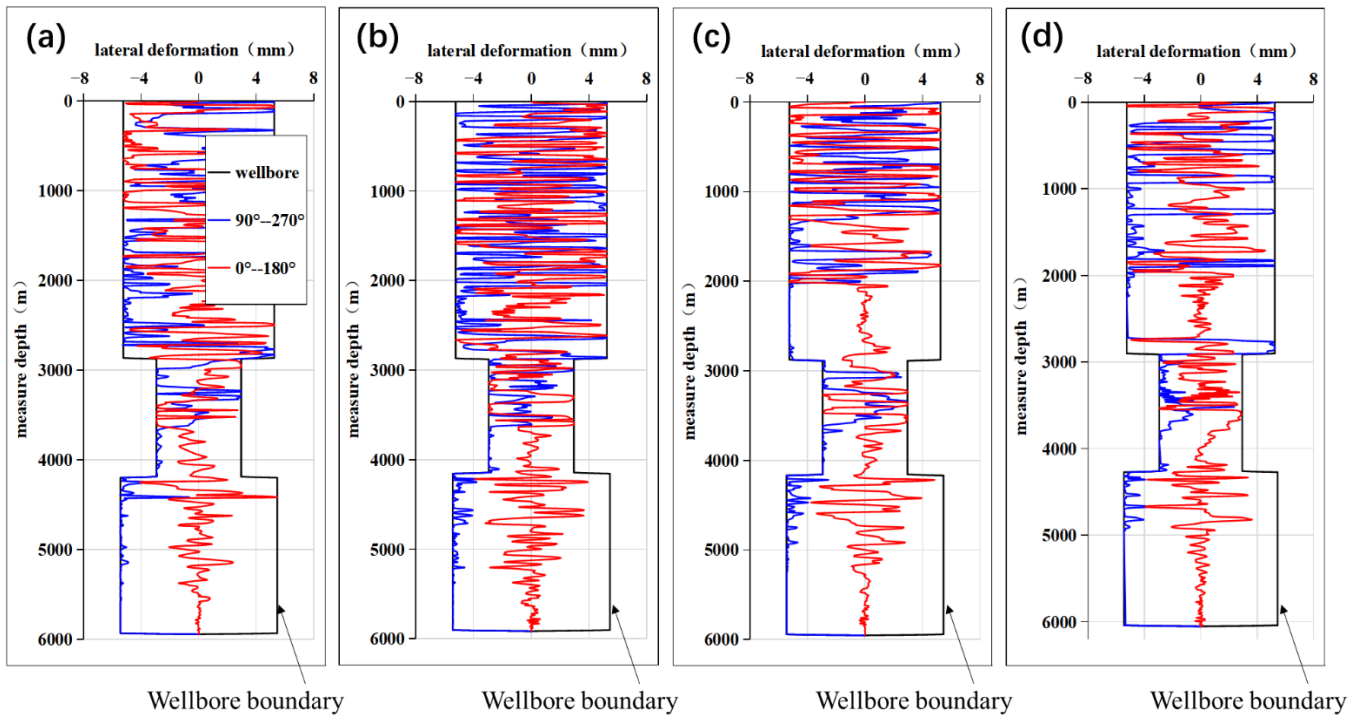


Figure 4. The lateral deformation displacement of casing strings in four wells vs. measured depth: (a) H2-1, (b) H2-2, (c) H2-3, (d) H2-4.

3.2. Passability

Figure 5 illustrates the schematic diagram of the tool passability calculation. In Figure 5, the radius of the borehole curvature is defined as R_1 , the diameter of the borehole is defined as D , the maximum outer diameter of the rigid downhole tool is defined as d_1 , the outer diameter of the pipe is defined as d_2 , and the minimum bending radius of the pipe is defined as R_2 . K_1 is the steel flexural safety factor, the parameter is set as 1.8 in API (American Petroleum Institute) regulations; K_2 is the stress concentration coefficient of the tool, the parameter is set as 3.0 in API.

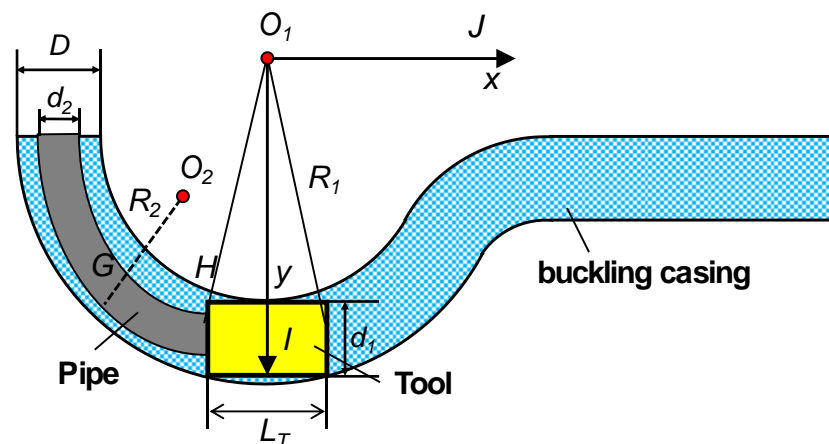


Figure 5. The schematic diagram of tool passability calculation.

The minimum bending radius of the pipe R_2 can be calculated as follows:

$$R_2 = \frac{DEK_1K_2}{\left[(\sigma_\theta + \sigma_r) + \sqrt{4\sigma_s^2 - 3(\sigma_\theta + \sigma_r)^2} \right]} \tag{2}$$

In Figure 5, $\overline{O_1J}$ is X axis, $\overline{O_1I}$ is Y axis, the geometric relationship can be expressed as:

$$|\overline{O_1A}| = R_1 - D/2 + d_1/2 \quad (3)$$

The coordinates of O_2 are $(\frac{L}{2}, |\overline{O_1I}| - R_2)$, the geometric relation of tangent between the casing string and the downhole tool can be illustrated as:

$$|\overline{O_1O_2}| = \sqrt{\left(\frac{L}{2}\right)^2 + (|\overline{O_1I}| - R_2)^2} \quad (4)$$

$$|\overline{O_1O_2}| + R_2 + \frac{d_2}{2} = R_1 + \frac{D}{2} \quad (5)$$

Substituting Equations (3) and (4) into Equation (5), the geometric relationship can be expressed as:

$$\begin{cases} L^2 = 8R_1(m+n) - 4m^2 + 4n^2 \\ m = D/2 - d_1/2 + R_2 \\ n = D/2 - R_2 - d_2/2 \end{cases} \quad (6)$$

The minimum length of the rigid downhole tool can be calculated as:

$$L = 2\sqrt{2R_1(m+n) - m^2 + n^2} \quad (7)$$

Meanwhile, the minimum radius of borehole curvature that the rigid downhole tool with a length L could pass is expressed as:

$$R_1 = \frac{L^2 + 4m^2 - 4n^2}{8(m+n)} \quad (8)$$

The above formulas could be used when the pipe is tangent to the borehole. If the rigid downhole tool is tangent to the borehole, the formula for calculating the minimum radius of the borehole curvature can be expressed as follows:

$$\begin{cases} R_1 = \frac{L^2 + 4m^2 - 4n^2}{8(m+n)}, |\overline{O_1H}| + \frac{d_1}{2} \leq R_1 + \frac{D}{2} \\ R_1 = \frac{L^2 + 4d_1^2 - 4Dd_1}{8(D-d_1)}, |\overline{O_1H}| + \frac{d_1}{2} > R_1 + \frac{D}{2} \end{cases} \quad (9)$$

Based on the theory of tool passability in a bending borehole (described in Figure 5), the passability of the downhole tool in the buckling casing could be obtained. Figure 6 illustrates the maximum allowable length of downhole tool in H2 platform (in this case, the passability test tool is the $\Phi 99$ cylinder), and the test tool is run from the wellhead to the bottom. It can be seen that the maximum allowable lengths of test tool in four wells are 5.2 m, 5.7 m, 4.8 m and 6.1 m, respectively. Significantly, according to the calculation results, it can be analyzed that: (i) the buckling deformation caused by running the casing string process is not sufficient to prevent the tool, (ii) there is no obvious relationship between casing buckling and CDBF, e.g., in the perspective of tool passability, the buckling degree of casing in the H2-2 well (un-CD) is not the lowest, but there is no CD phenomenon. Meanwhile, the degree of casing in the H2-4 well (CD) is the least. In conclusion, according to the tubular mechanical calculation of casing string, due to the action of centralizers, the buckling deformation of casing string is acceptable for tool passage (only ± 5.5 mm along lateral direction), and the bridge plug with conventional size ($\Phi 99$ mm) could not be obstructed in the buckling casing string during the running in process.

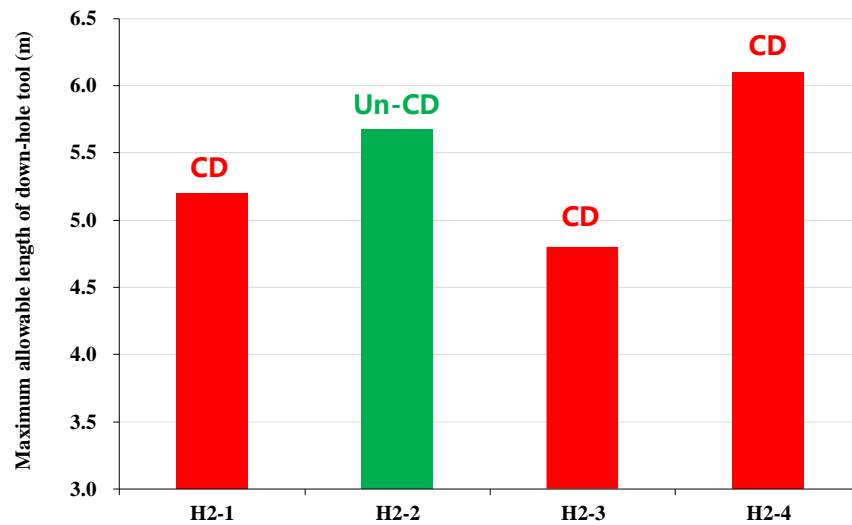


Figure 6. The maximum allowable length of downhole tool in the H2 platform.

4. Analysis of Geological Factors

4.1. Formation Fracture/Fault

Figure 7 illustrates the vertical fractures/faults distribution diagram of the H2 platform in the shale reservoir. It can be seen that there are several CD positions coincident with the vertical fractures/faults, e.g., F1 region in H2-1 well and F2 region in H2-3 well. However, the correlation between CD positions and vertical fractures/faults is not high, according to the statistical data in Figure 7. Significantly, there are 6 CD positions are not in the vertical fractures/faults in H2-3 well and H2-4 well; among these CDs, the maximum CD degree reaches 18%. Moreover, all CD points are positioned close to A location; correspondingly, there is no CD positions near point B, although there are many formation fracture/faults in the region near point B.

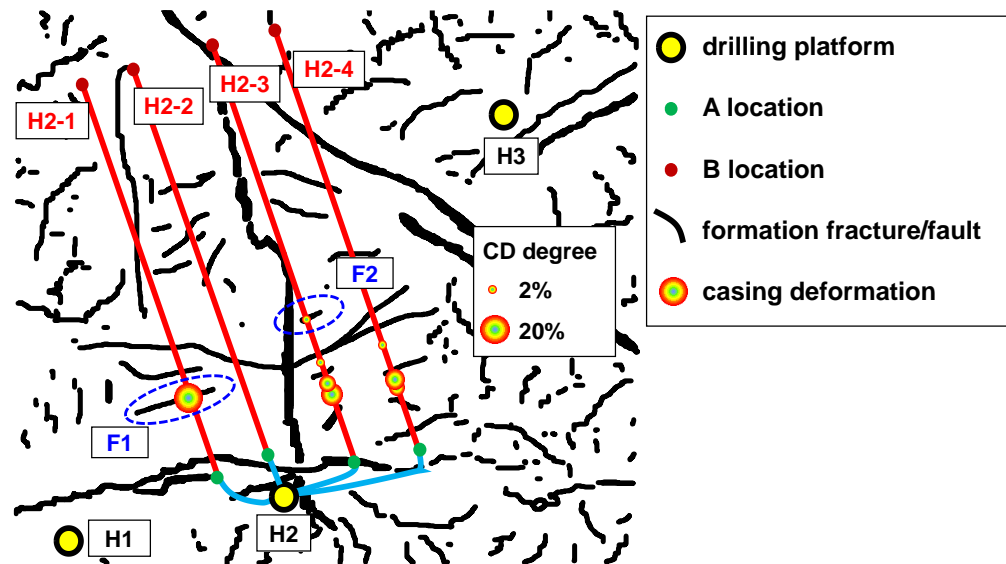


Figure 7. The vertical fractures/faults distribution diagram of H2 platform in the shale reservoir.

4.2. Horizontal Formation Layer Slip

Figure 8 shows the comparison diagram of actual casing trajectory and reservoir rock in the horizontal section in the H2 platform: (a) H2-1, (b) H2-2, (c) H2-3, (d) H2-4. The target reservoir is S#1 and its lithology is shale. Adjacent to S#1 are the formations S#2, S#3 and M#1, where S#2 and S#3 are shales (with different rock parameters from S#1, including porosity, permeability and acoustic transmission rate, etc.) and M#1 comprises

massive carbonate rocks. There are casings in the horizontal section of four wells through layers of different lithologies, back and forth. In the H2-1 well, all the CD positions are at the f vertical formation fracture/fault (Figure 8a). However, in the H2-3 well, horizontal formation layer slip is the main cause of CD, and the CD positions are mostly at the interface between M#1 and S#1 (Figure 8c). Meanwhile, in the H2-3 and H2-4, all CD positions are at the interface between M#1, S#1 and S#2 (Figure 8d). Through the comparison between the CD positions and the geological stratification (horizontal and vertical), a preliminary analysis can be obtained: (i) the main cause of CD is geological activity, and (ii) geological activity includes vertical formation fractures/faults and horizontal formation layer slip, in which the horizontal formation layer slip is more dominant.

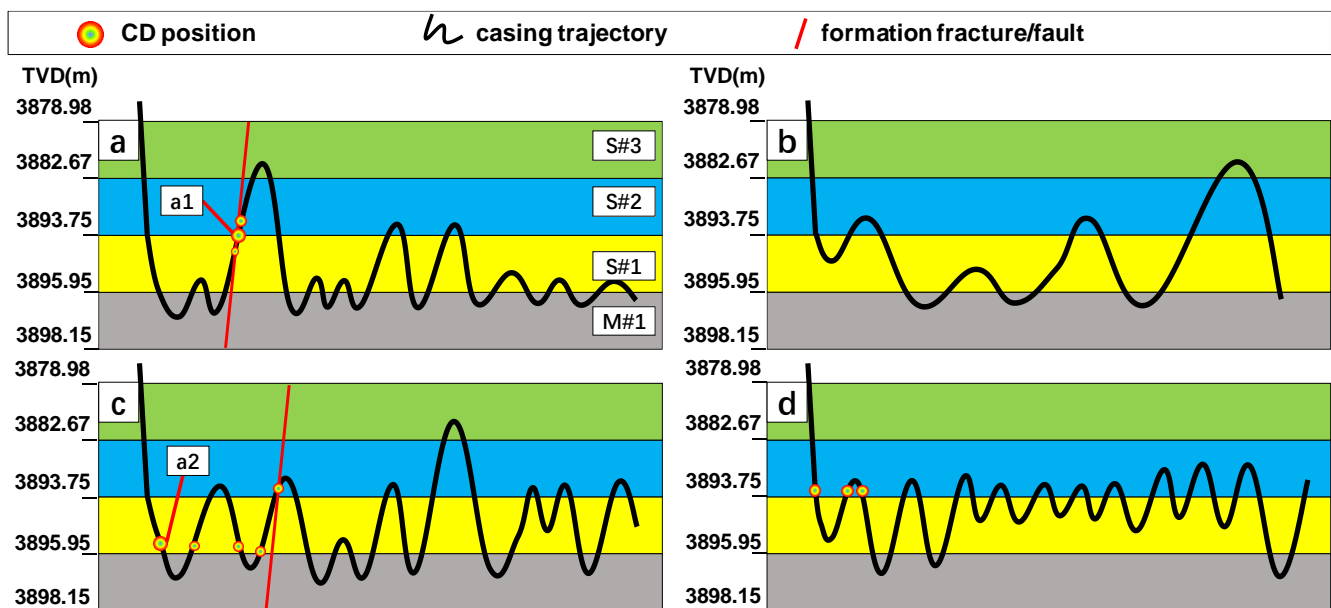


Figure 8. The comparison diagram of actual casing trajectory and reservoir rock in a horizontal section in the H2 platform: (a) H2-1, (b) H2-2, (c) H2-3, (d) H2-4.

4.3. Modeling

In order to further verify the preliminary conclusion of the analysis, two sets of CD positions are analyzed in detail: a1 (described in Figure 8a, 4356.01 m~4356.49 m, in vertical fracture/fault) and a2 (described in Figure 8c, 4146.36 m~4149.07 m, in horizontal formation layer slip).

An interesting phenomenon is that due to different geological migration mechanisms, the length of the CD varies significantly. Figure 9 illustrates the casing inner diameter logging results. It can be seen that: (i) the CD length in a2 is 5.64 times that of a1 (the CD length in a1 is 0.48 m, the CD length in a2 is 2.71 m), (ii) the CD morphology in a1 and a2 is typical shear deformation. The well logging results are obtained by a multi-finger image tool (MIT), consisting of electronic circuit, electric motor, 24-arm borehole diameter measuring probe and other components.

According to the logging results, it can be preliminarily analyzed that in a1, the angle between the vertical fractures surface and the casing axial direction is almost 45° (as calculated through the actual casing trajectory and geological lithology) when the formation slips, so the length of CD is relatively short. However, in a2, the angle between the horizontal formation layer surface and the casing axial direction is only 3.73° (as calculated through actual casing trajectory and geological lithology), so the length of CD is relatively long.

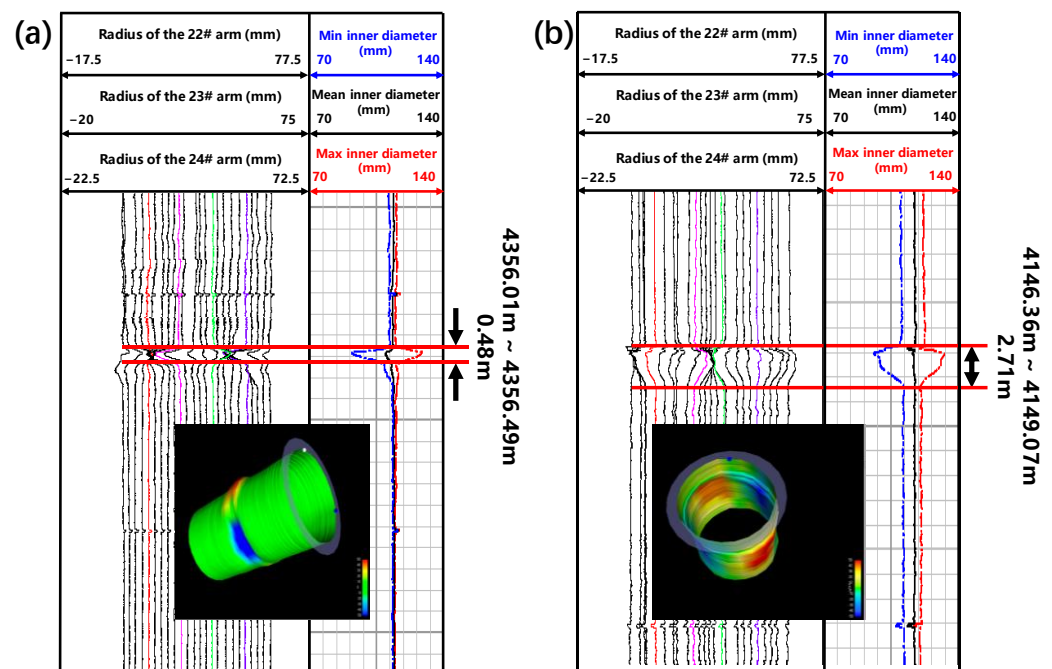


Figure 9. The casing inner diameter logging results: (a) CD position (well depth 4356.01 m~4356.49 m) in H2-1 well, (b) CD position (well depth 4146.36 m~4149.07 m) in H2-3 well.

In order to verify the CD mechanism analyzed based on logging results, two groups of FE models are established to reduce the CD process: CD mechanism in a1 and a2. The CD FE model in a1 is shown in (i) modeling: the coupling FE model consists of casing ($\Phi 139.7 \text{ mm} \times \text{wall } 12.7 \text{ mm} \times 10 \text{ m}$, steel degree 140 ksi, elasticity modulus 210 GPa, poisson's ratio 0.3), cement ($\Phi 215.9 \text{ mm} \times \text{wall } 38.1 \text{ mm} \times 10 \text{ m}$, elasticity modulus 20 GPa, poisson's ratio 0.25), and rock (it is divided into two parts by the 45° formation fracture, and the size of the rock is $2 \text{ m} \times 2 \text{ m} \times 10 \text{ m}$ when the two parts are combined, elasticity modulus 43.5 GPa, poisson's ratio 0.25), and contact relationships between each component is established; (ii) initial geostress: the vertical geostress is 91 MPa, the horizontal maximum geostress is 96 MPa, the horizontal minimum geostress is 87 MPa, and the axial direction of the casing is along the direction of the minimum horizontal principal geostress; (iii) displacement loading: one rock part is fixed, another rock part slips along the 45° formation fracture, and the slip displacement is 40 mm.

Simultaneously, the CD FE model in a2 is shown in Figure 10b: (i) modeling: the coupling FE model consists of casing ($\Phi 139.7 \text{ mm} \times \text{wall } 12.7 \text{ mm} \times 45 \text{ m}$, 140 ksi steel degree), cement ($\Phi 215.9 \text{ mm} \times \text{wall } 38.1 \text{ mm} \times 45 \text{ m}$), and rock (it is divided into two parts by the horizontal formation layer, and the size of the rock is $2 \text{ m} \times 2 \text{ m} \times 45 \text{ m}$ when the two parts are combined), and contact relationships between each component is established; (ii) loading: one rock part is fixed, and another rock part slips along the horizontal formation interface, and the slip displacement is 40 mm. The comparison diagram shows the actual casing trajectory and reservoir rock in the horizontal section in the H2 platform.

4.4. Simulation Results

Figure 11 describes the von Mises stress contour of CD casings due to vertical formation fractures/faults slip type and horizontal formation layer slip type. It can be seen that the length of the high stress zone of the CD casing due to the horizontal formation layer slip (a1) is significantly longer than that of the casing due to the vertical formation fractures/faults slip (a2) (the length of CD casing in a1 is only 0.435 m, but the length of CD casing in a2 reaches 2.519 m). The results of this simulation are in good agreement with the logging results in Figure 9 (the length of CD casing is 0.48 m in a1, and the length of CD casing is

2.71 m in a2). Moreover, the distribution of plastic deformation regions (stress ≥ 965 MPa (140 ksi)) is also different for the two types of CD.

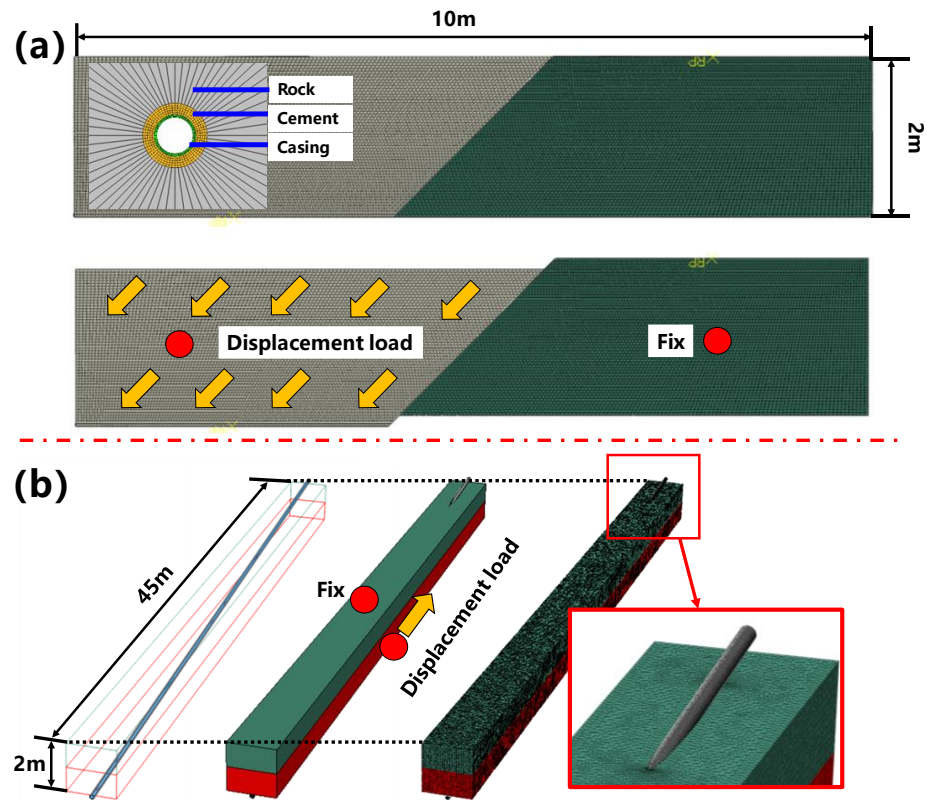


Figure 10. Two groups of FE models coupled casing—cement—rock considering the slip of the formation: (a) CD mechanism in a1, (b) in a2.

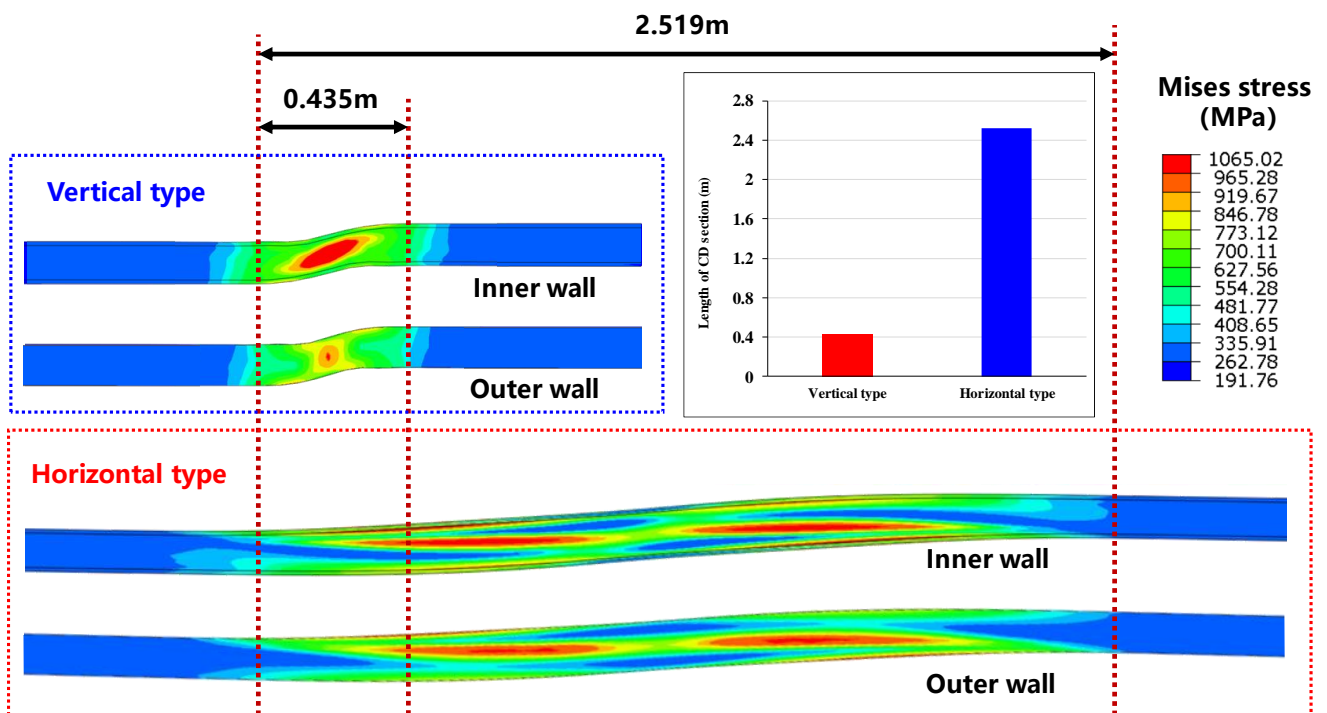


Figure 11. The von Mises stress contour of CD casing due to vertical formation fractures/faults slip type and horizontal formation layer slip type.

Table 2 presents the comparison of all the CD logging data and the FE simulation in the H2-3 well. It can be seen that this is consistent with our hypothesis. The numerical simulation results (high stress section length from FE model) are in good agreement with the actual CD logging results in No. 1~No. 4 CD positions (logging results—FE results: 2.71–2.51, 3.5–2.86, 4.92–4.68, 2.14–2.11). Moreover, the smaller the angle of casing-formation layer, the longer the CD length. The calculated results (2.99 m) of CD length of No. 5 position through the lateral formation slip model (Figure 10b) are not consistent with the actual logging results (0.87 m). However, the calculated results (0.67 m) are in good agreement with the actual logging results (0.87 m) when the vertical formation fractures/faults slip model (Figure 10a), the angle between the vertical fracture surface and the casing axial direction is 31° is used. Apparently, these results confirm well the preliminary conclusion that lateral formation slip is the main cause of CD (Figure 11).

Table 2. The comparison of all the CD logging data and the FE simulation in the H2-3 well.

No.	CD Section Depth (m)	Angle of Casing-Formation Layer ($^\circ$)	CD Section Length from Logging Results (m)	High Stress Section Length from FE Model (m)
1	4146.36–4149.07	3.73	2.71	2.51
2	4269.99–4273.49	3.42	3.5	2.86
3	4373.04–4377.96	1.72	4.92	4.68
4	4399.85–4401.99	3.99	2.14	2.11
5	4605.50–4606.37	3.27	0.87	0.67/2.99

Figure 12a illustrates the number of casing passes through the different horizontal lithologic layers (TL). It can be found from the data that the number of TL of CD wells is significantly higher (the casing in H2-1 well is 31 times, H2-3 is 31 times and H4-1 is 23 times); however, H2-2 is only 16 times. This phenomenon that CD wells have a higher number of TL is also typical in other platforms. Figure 12b shows the number of CD position in the H2 platform due to TL and TF (through the vertical formation fractures/faults); it can be seen from the data that 66.67% of the CD positions in H2 platform are caused by TL. In practice, based on the actual data, among the 85 CD positions in L oilfield, 60 CD positions are caused by TL (70.58%), 8 CD positions are caused by TF (9.42%), and the cause of 17 CD positions is unknown (20.00%). It can be analyzed that the greater the number of TL, the greater the probability of CD. Moreover, according to the data of the relationship between CD and TL, the TL is the main cause of CD. Through the above analysis, it can be seen that both TL and TF could cause CD, and TL is the main reason for it. Therefore, in the process of drilling, reducing the number of TL of the well trajectory could effectively reduce the probability of CD.

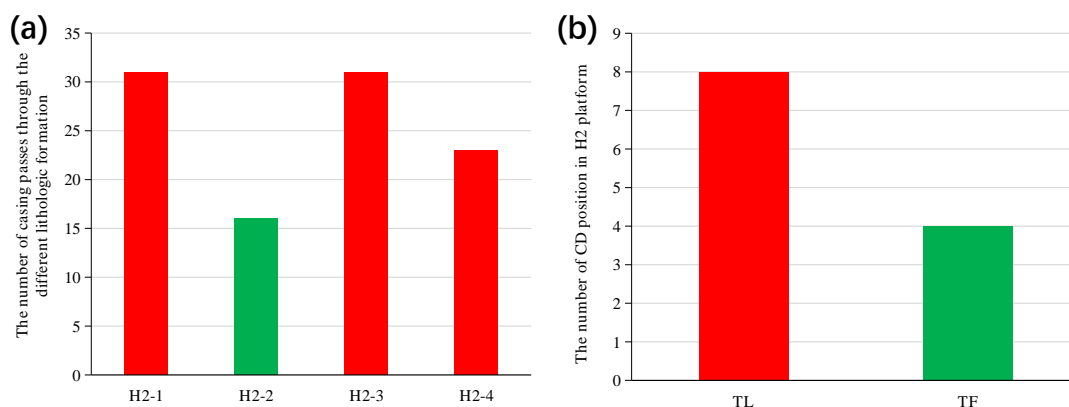


Figure 12. The statistics of CD positions: (a) the number of casing passes through the different horizontal lithologic layers, (b) the number of CD positions in the H2 platform due to different reasons (TL and TF).

5. The Phenomenon of CD Positioning Close to a Point of Wells

Based on the statistical results of CD positions for 60 CD wells in the L field, more than 90% of the CD positions are at a point on the A-C path (assume that the midpoint between point A and point B is defined as point C). Apparently, the statistical results of CD positions in the wells of H2 platform are also in good agreement with this phenomenon; all CD positions are located in the A-C path. It is well known that when a string bends or buckles, its residual strength could decrease to some extent; meanwhile, when a string is subjected to axial force, its residual strength could also decrease. Correspondingly, it can be seen from Figure 4 that casing buckling in sections A-C is more severe than that in C-B sections. On the other hand, for the casing in a horizontal shale gas well, the axial force in the horizontal section of the string is usually compressive axial force, and the axial force is larger as it is closer to point A. Therefore, based on the calculation of the fourth strength theory [25], it can be found on a preliminary basis that the residual strength of casing could decrease when it is close to point A, and the casing with lower residual strength could be more prone to deformation due to geological reasons. Figure 13 illustrates the percentage of casing residual collapse resistance in four wells vs. measured depth (H2 platform, along A-B section). It can be seen from Figure 13 that: (i) in the A-B section, the residual strength of the four casing strings increases nonlinearly along the measured depth, (ii) the residual strength of the casing in the H2-2 well is significantly higher than that of the other three wells, (iii) all CD positions are at faults (vertical fracture surface and the horizontal formation layer surface) in dense region I. Therefore, it can be analyzed that the phenomenon that many CD positions are close to point A of wells is caused by the comprehensive influence of the tubular mechanical and geological factors.

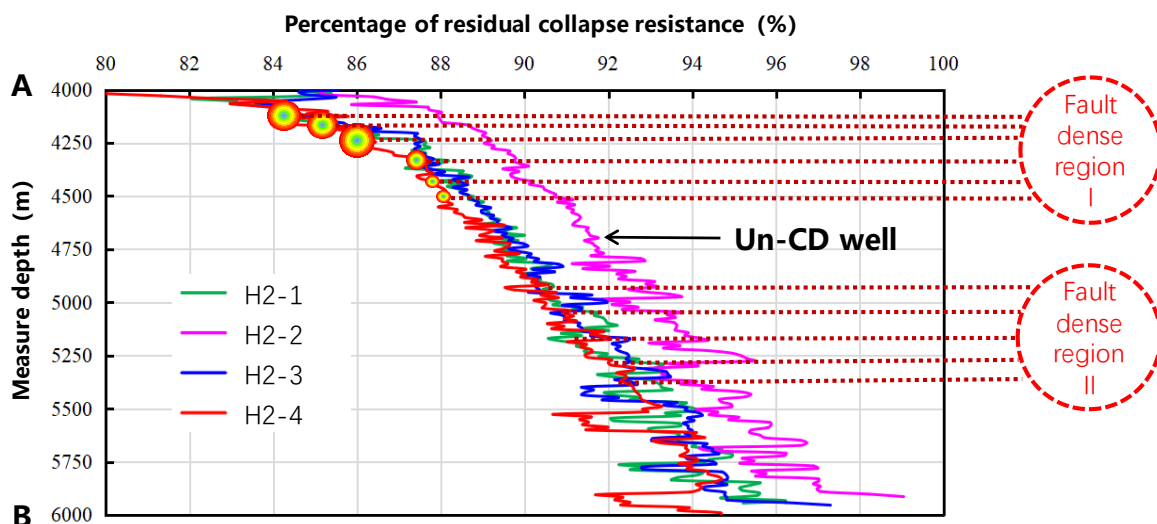


Figure 13. The percentage of casing residual collapse resistance in four wells vs. measured depth (H2 platform, along A-B section).

6. Discussion

According to the tubular mechanical calculations for the casing string, due to the action of centralizers, the buckling deformation of the casing string is acceptable for downhole tool passage (only ± 5.5 mm along lateral section), and the bridge plug with conventional size ($\Phi 99$) could not be obstructed in the buckling casing string during running in. Moreover, since the fracturing process has been completed on platforms H1 and H3, the formation on H2 platform has the prerequisites to be activated. It can be analyzed that the working fluid used in the fracturing process of the H1 and H3 platforms entered the formation of the H2 platform, resulting in the decrease of the friction resistance between the interfaces of vertical fractures and the horizontal layers of the formation in the H2 platform, and finally causing the formation slip. The formation activation area is mainly distributed near the

reservoir (S#1, S#2, S#3 and M#1) according to the research results. Further, according to the statistics of field data and FE calculation results, geological factors are the main cause of CD, among which the horizontal formation layer slip is the main factor and the vertical fracture/fault slip is the secondary factor. However, according to the statistics of the CD positions, most of the CD positions are distributed in the A-C section (66.67%). This is because the residual strength of the casing in the A-C section is lower than that of the casing in the C-B section. The difference in strength is due to various factors: (i) casing buckling in sections A-C is more serious, and additional buckling stress reduces the residual strength of casing; (ii) due to the wellbore trajectory of horizontal wells, the compressive axial force of casing in sections A-C is significantly larger than that of casing in sections C-B. Obviously, it is well known that vertical fractures/faults in shale reservoirs are very dense, based on the density of fractures/faults distribution in the reservoir. Thus, vertical fractures/faults are unavoidable in the wellbore trajectory when the target layer is determined. Fortunately, vertical fractures are not the main factor of CD in L field. From the engineering perspective, the number of CD positions could be reduced by: (i) avoiding frequent TL of the wellbore trajectory, (ii) optimizing the casing running in process (rotational speed, sitting weight of casing at wellhead) to reduce buckling and improve casing residual strength.

7. Conclusions

- (1) According to the tubular mechanical calculation of casing string, due to the action of centralizers, the buckling deformation of casing string is acceptable for tool passage (only ± 5.5 mm along lateral section), and the bridge plug with conventional size ($\Phi 99$) could not be obstructed in the buckling casing string during string running in.
- (2) According to the statistics of field data and FE calculation results, geological factors are the main cause of CD, among which the horizontal formation layer slip is the main factor and the vertical fracture/fault slip is the secondary factor.
- (3) The phenomenon that many CD positions are close to point A of wells is caused by the comprehensive influence of the tubular mechanical and geological factors.
- (4) From the engineering perspective, the number of CD positions could be reduced by: (i) avoiding frequent TL numbers in the wellbore trajectory, and (ii) optimizing the casing running in process (rotational speed, sitting weight of casing at wellhead) to reduce buckling and improve casing residual strength.

Author Contributions: Y.M.: Methodology, Investigation, Writing—original draft; J.C.: Conceptualization, Resources, Writing—review and editing; J.W.: Formal analysis, Validation, Investigation, Funding acquisition; F.W.: Writing—review and editing, Investigation; M.T.: Conceptualization, Resources, Writing—review and editing; L.H.: Validation, Investigation. All authors have read and agreed to the published version of the manuscript.

Funding: The authors would like to gratefully acknowledge the supports of Scientific Research and Technology Development of CNPC (2021DJ2705, 2021DJ4403, 2020B-4020), the Innovative Talents Promotion Program—Young Science and Technology Nova Project (2021KJXX-63) and the Study on key technology of stimulation and modification for Gulong shale oil (2021ZZ10-04).

Institutional Review Board Statement: Not applicable.

Informed Consent Statement: Not applicable.

Data Availability Statement: Not applicable.

Conflicts of Interest: The authors declare that there are no conflict of interest.

Nomenclature

R_1	radius of curvature of the well-hole	m
D	diameter of the well-hole	m
d_1	maximum outer diameter of the rigid downhole tool	m
d_2	outer diameter of the pipe	m
R_2	minimum bending radius of the pipe	m
K_1	steel flexural safety factor	/
K_2	stress concentration coefficient of the tool	/
L	rigid downhole tool length	m
m	process coefficient	m
n	process coefficient	m
E	elasticity modulus	Pa
σ_θ	hoop stress of tool	Pa
σ_r	radial stress of tool	Pa
σ_s	axial stress of tool	Pa
ΔF_{all}	total change of internal force in tubing	N
ΔF_1	force change from friction effect	N
ΔF_2	force change from buckling effect	N
ΔF_3	force change from friction effect due to fluid flow	N
ΔF_4	force change from ballooning effect	N
ΔF_5	force change from piston effect	N

References

- Mou, Y.; Lian, Z.; Sang, P.; Yu, H.; Zhang, Q.; Li, R. Study on water hammer effect on defective tubing failure in high pressure deep gas well. *Eng. Fail. Anal.* **2019**, *106*, 104154. [\[CrossRef\]](#)
- Mou, Y.; Lian, Z.; Lin, T.; Zhang, Q.; Liu, Y. Study on Fatigue of Tubing Joint Thread Induced by Vibration in HTHP Ultradeep Wells. *J. Press. Vessel. Technol.* **2020**, *142*, 031502. [\[CrossRef\]](#)
- Zhao, J.; Ren, L.; Jiang, T.; Hu, D.; Wu, J.; Yin, C.; Hu, Y.; Lin, R. Ten years of gas shale fracturing in China: Review and prospect. *Nat. Gas Ind. B* **2022**, *9*, 158–175. [\[CrossRef\]](#)
- Kirat, Y. The US shale gas revolution: An opportunity for the US manufacturing sector? *Int. Econ.* **2021**, *167*, 59–77. [\[CrossRef\]](#)
- Omari, A.; Wang, C.; Li, Y.; Xu, X. The progress of enhanced gas recovery (EGR) in shale gas reservoirs: A review of theory, experiments, and simulations. *J. Pet. Sci. Eng.* **2022**, *213*, 110461. [\[CrossRef\]](#)
- Heider, Y. A review on phase-field modeling of hydraulic fracturing. *Eng. Fract. Mech.* **2021**, *253*, 107881. [\[CrossRef\]](#)
- Zhang, X.; Li, J.; Lian, W.; Wang, Z.; He, L.; Liu, W. Research on casing deformation mechanism and prevention measures based on micro-seismic signal distribution. *J. Pet. Sci. Eng.* **2022**, *217*, 110874. [\[CrossRef\]](#)
- Yu, H. *Study on Casing Failure Mechanism in Volumetric Fracturing Process*; Southwest Petroleum University: Chengdu, China, 2015.
- Chen, C.; Shi, L.; Xiang, D. Mechanism and countermeasures of casing deformation in the Changning-Weiyuan shale gas demonstration area. *Nat. Gas Ind.* **2016**, *36*, 70–75. [\[CrossRef\]](#)
- Daneshy, A. Impact of off-balance fracturing on borehole stability and casing failure. In Proceedings of the SPE-93620-MS, Presented at the SPE Western Regional Meeting, Irvine, CA, USA, 30 March–1 April 2005.
- Sugden, C.; Johnson, J.; Chambers, M.; Suryanarayana, P. Special Considerations in the Design Optimization of the Production Casing in High-Rate, Multistage-Fractured Shale Wells. *SPE Drill. Complet.* **2012**, *27*, 459–472. [\[CrossRef\]](#)
- Lian, Z.; Yu, H.; Lin, T.; Guo, J. A study on casing deformation failure during multi-stage hydraulic fracturing for the stimulated reservoir volume of horizontal shale wells. *J. Nat. Gas. Sci. Eng.* **2015**, *23*, 538–546. [\[CrossRef\]](#)
- Li, L.; Wang, G.; Lian, Z.; Zhang, L.; Mei, J.; He, Y. Deformation mechanism of horizontal shale gas well production casing and its engineering solution: A case study on the Huangjinba Block of the Zhaotong National Shale Gas Demonstration Zone. *Nat. Gas Ind. B* **2017**, *37*, 91–99. [\[CrossRef\]](#)
- Yan, W.; Zou, L.; Li, H.; Deng, J.; Ge, H.; Wang, H. Investigation of casing deformation during hydraulic fracturing in high geo-stress shale gas play. *J. Pet. Sci. Eng.* **2017**, *150*, 22–29. [\[CrossRef\]](#)
- Fei, Y.; Yang, X.; Han, L.; Wu, X. Quantifying the induced fracture slip and casing deformation in hydraulically fracturing shale gas wells. *J. Nat. Gas Sci. Eng.* **2018**, *60*, 103–111.
- Xi, Y.; Li, J.; Zha, C.; Guo, B.; Liu, G. A new investigation on casing shear deformation during multistage fracturing in shale gas wells based on microseism data and calliper surveys. *J. Pet. Sci. Eng.* **2019**, *180*, 1034–1045.
- Guo, X.; Li, J.; Liu, G.; Yan, X.; Zeng, Y.; Miao, H.; Hui, Y. Numerical simulation of casing deformation during volume fracturing of horizontal shale gas wells. *J. Pet. Sci. Eng.* **2019**, *172*, 731–742. [\[CrossRef\]](#)
- Holt, R.; Larsen, I.; Fjr, E.; Stenebrten, J. Comparing mechanical and ultrasonic behaviour of a brittle and a ductile shale: Relevance to prediction of borehole stability and verification of shale barriers. *J. Pet. Sci. Eng.* **2019**, *187*, 106746. [\[CrossRef\]](#)

19. Li, H.; Li, Z.; Li, G.; Yu, H.; Jiang, Z.; He, L.; Guo, B.; Dong, M. Casing deformation mechanisms of horizontal wells in Weirong shale gas field during multistage hydraulic fracturing. *J. Nat. Gas Sci. Eng.* **2020**, *84*, 103646. [[CrossRef](#)]
20. Ajayi, K.; Schatzel, S. Transport model for shale gas well leakage through the surrounding fractured zones of a longwall mine. *Int. J. Min. Sci. Technol.* **2020**, *30*, 635–641. [[CrossRef](#)] [[PubMed](#)]
21. Yang, S.; Han, L.; Wang, J.; Wu, X. Laboratory study on casing deformation during multistage horizontal well fracturing in shale gas development and strain based casing design. *J. Nat. Gas Sci. Eng.* **2021**, *89*, 103893. [[CrossRef](#)]
22. Mohammed, A.; Bartlett, M.; Oyeneyin, B.; Kayvantash, K.; Njuguna, J. An application of FEA and machine learning for the prediction and optimisation of casing buckling and deformation responses in shale gas wells in an in-situ operation. *J. Nat. Gas Sci. Eng.* **2021**, *95*, 104221. [[CrossRef](#)]
23. Lu, Q.; Liu, Z.; Guo, J.; He, L.; Li, Y.; Zeng, J.; Ren, S. Hydraulic fracturing induced casing shear deformation and a prediction model of casing deformation. *Pet. Explor. Dev.* **2021**, *48*, 460–468. [[CrossRef](#)]
24. Mou, Y.; Yang, S.; Han, L.; Wang, J.; Lian, Z. Mechanical Behavior and Optimization of Tubing String with Expansion Joint during Fracturing in HTUHP Wells. *Processes* **2022**, *10*, 1063. [[CrossRef](#)]
25. Mou, Y.; Lian, Z.; Yu, H.; Lin, T.; Han, Z.; Zhang, Q. SCC evaluation of composite materials for natural gas absorber based on experiment. *Eng. Fail. Anal.* **2020**, *110*, 104450. [[CrossRef](#)]